Supplementary

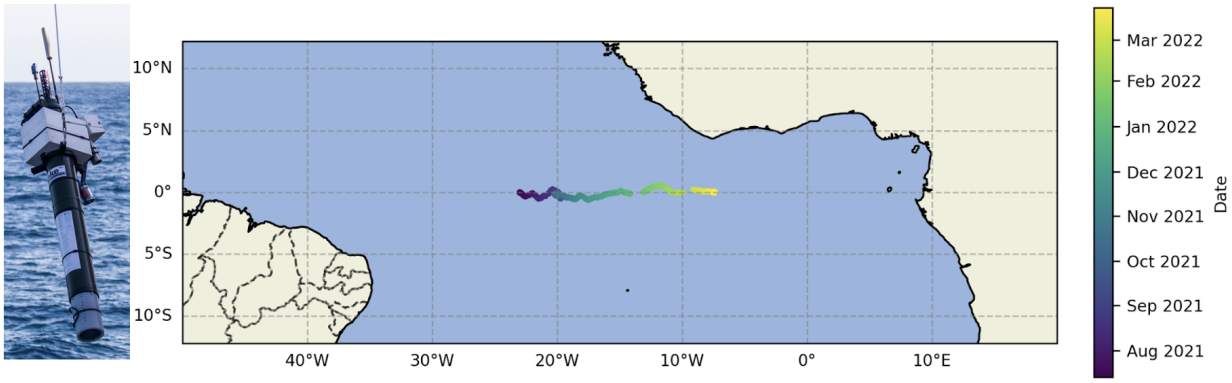

Figure S1: Photo of the BGC-Argo float with UVP6 taken by Knut Heinatz (left panel), Trajectory of the float along the equator (right panel), time is indicated as a color.

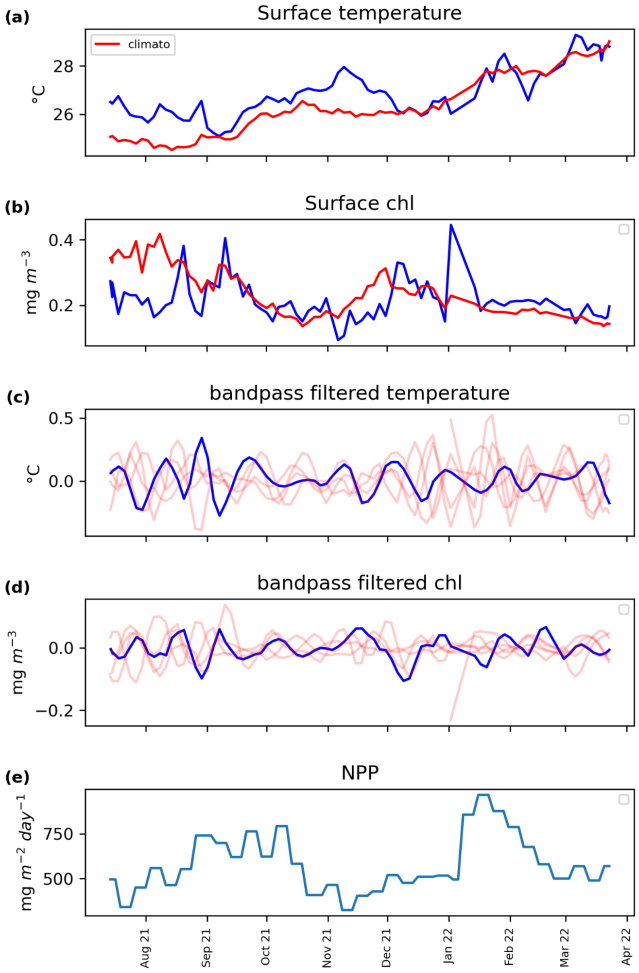

Figure S2: Satellite-derived (a) sea surface temperature, (b) chlorophyll a, (c) bandpass-filtered sea surface temperature anomaly, and (d) bandpass-filtered chlorophyll anomaly along the BGC Argo float trajectory. (e) Net Primary Production (NPP). Blue line: data extracted along the actual float trajectory. Red lines in (a) and (b): climatology from 2012 to 2022 extracted along the identical virtual trajectory started in July of each year. The transparent red lines in (c) and (d) show the annual variation of the bandpass-filtered temperature and chlorophyll anomalies.

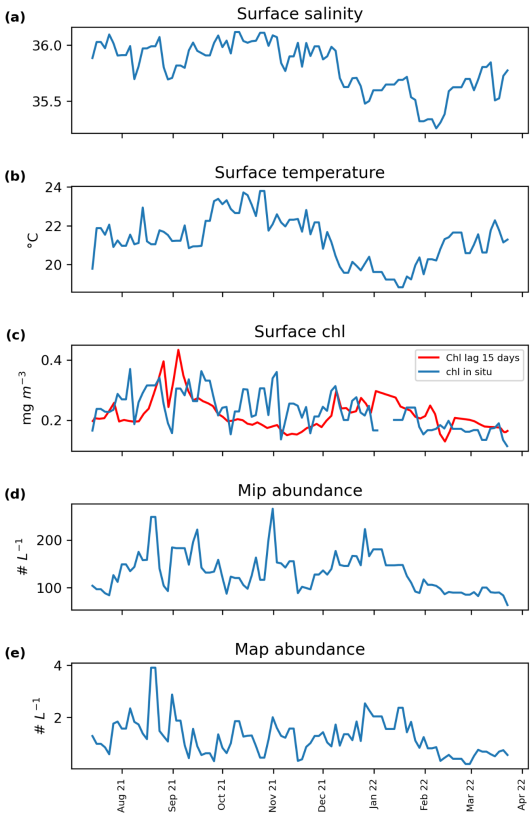

Figure S3: Mean float sensor data for the top 100 m surface layer along the BGC Argo float trajectory: (a) salinity, (b) temperature, (c) in situ chlorophyll (mg m^{-3}) and the Lagrangian chlorophyll for an advective time of 15 days (d) MiP abundance (# L^{-1}), (e) MaP abundance (# L^{-1}).

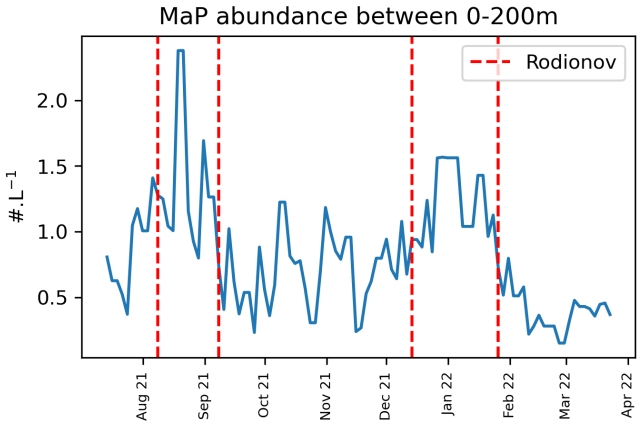

Figure S4: Times series of the MaP abundance for the layer between 0-200 m. The red dashed lines denote shifts detected by the sequential Rodionov algorithm.

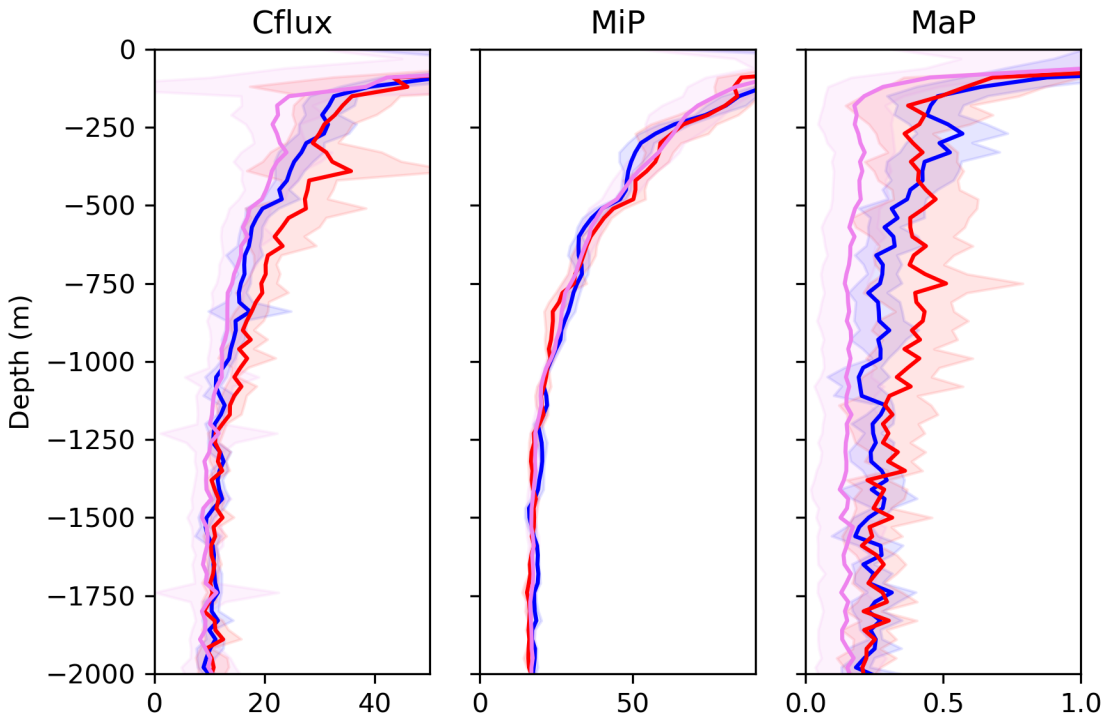

Figure S5: Averaged carbon flux profiles (mg C m^{-3}), MiP (# L^{-1}) and MaP (# L^{-1}) abundance along the water column, during event 1 (blue), event 2 (red), and the outside-between mask (purple) from 0-2000 m. The shading represents the standard deviation.

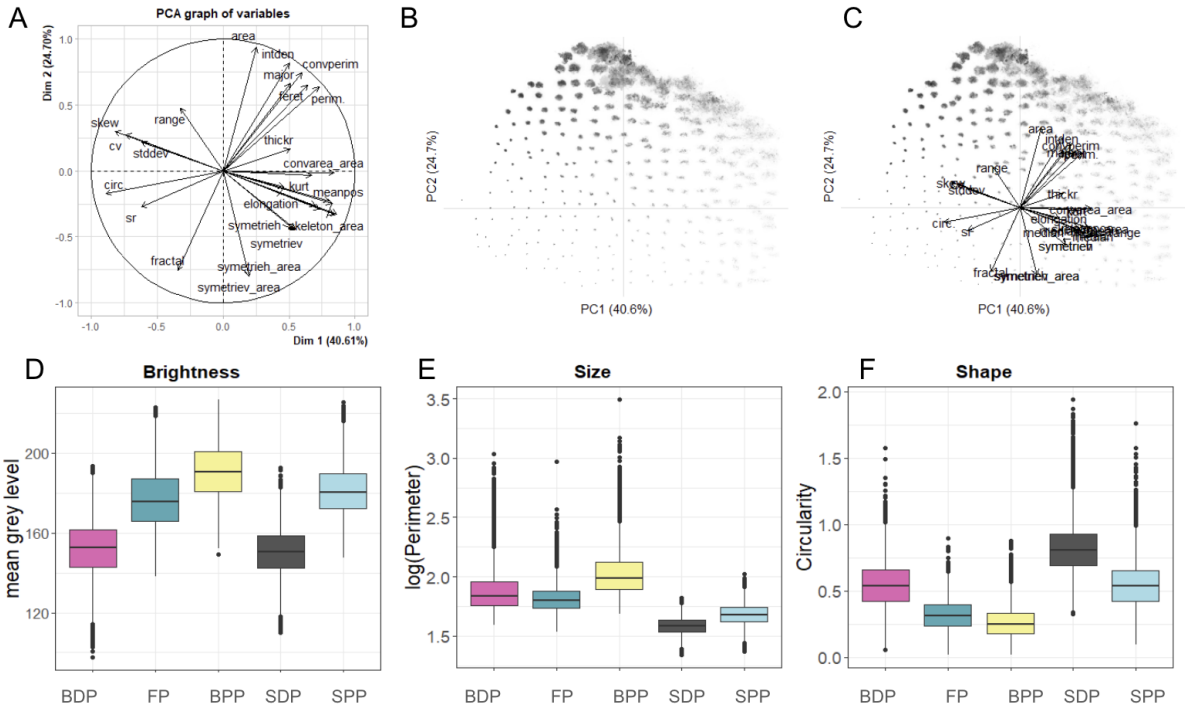

Figure S6 A. PCA graph of variables representing the 24 morphological characteristics of individual marine particles (arrows) B. PCA graph with the exemplary appearance spread over the 1st and 2nd axis C. Combination of the morphological characteristics and their images. Box plots of the mean values of key exemplary morphological properties characterizing the 5 morphotypes D. Brightness, E. Size, F. Shape

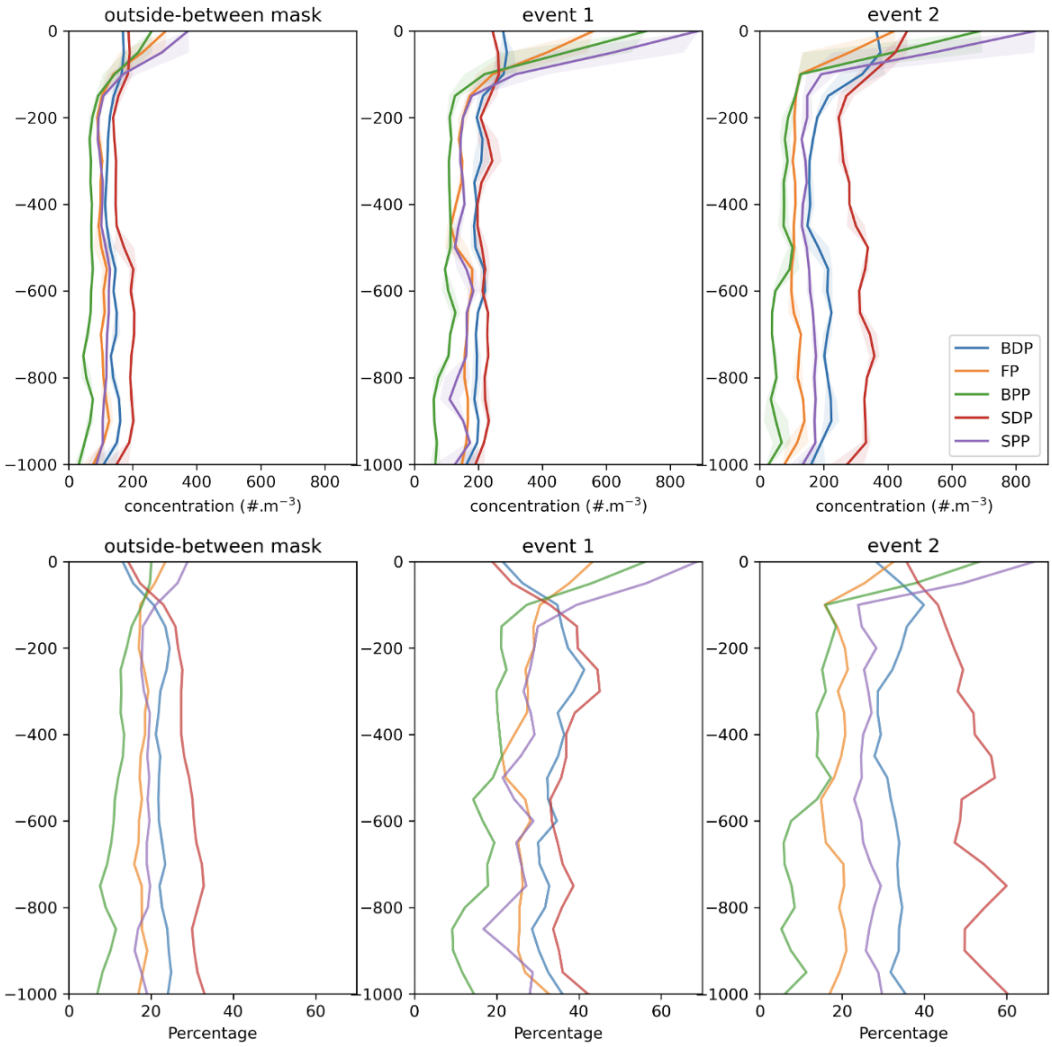

Figure S7 Averaged concentration profiles (# m^{-3}) and percentage (second row) of the different morphotypes along the plume, during the outside-between mask, event 1, and event 2.

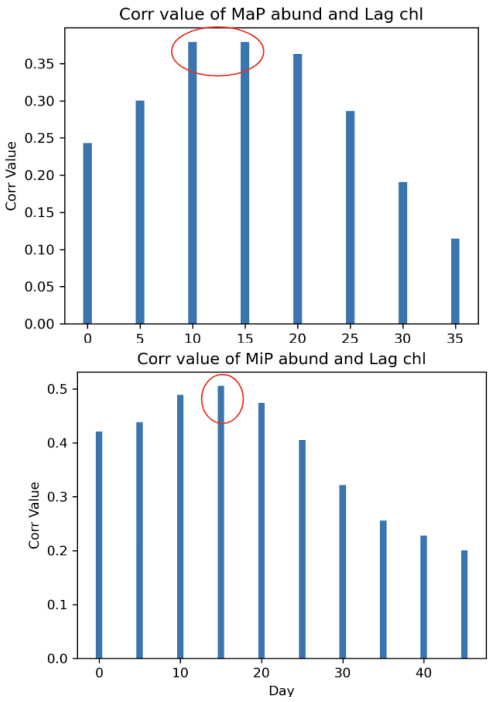

Figure S8 Correlations between Lagrangian chlorophyll of different advective times and MiP and MaP integrated between 0-100m.

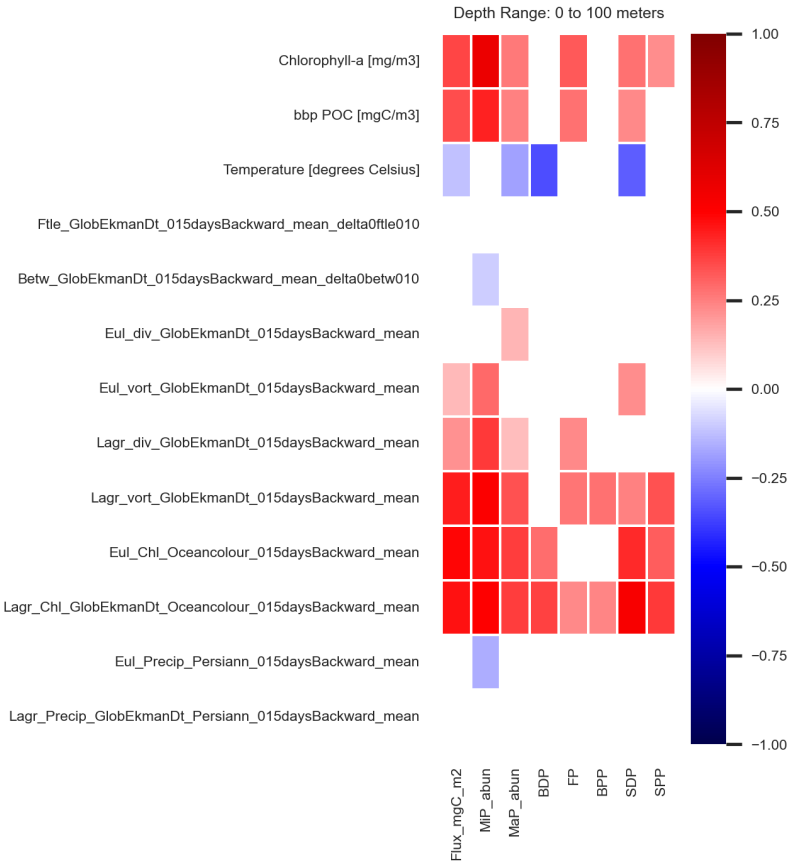

Figure S9 Correlations of the carbon flux, MiP, MaP, and cluster abundance in the first 100 m with the Lagrangian diagnostics and in situ data. Cluster 1: BDP, cluster 2: FP, cluster 3: BPP, cluster 4: SDP and cluster 5: SPP.

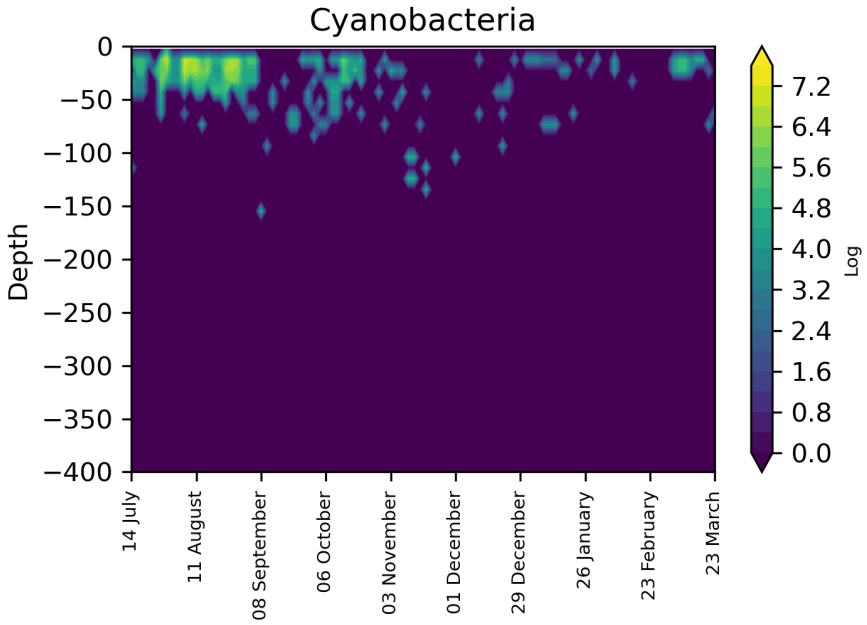

Figure S10 Time series of the logarithmic concentration of cyanobacteria (trichodesmium)

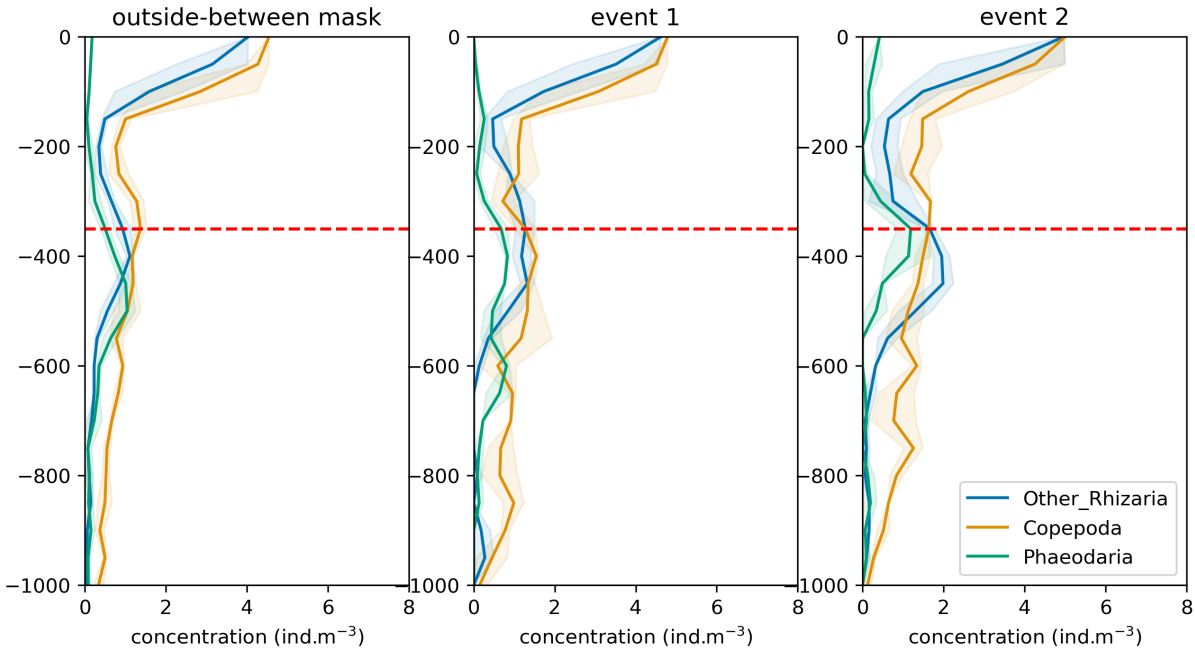

Figure S11 Profiles of the log concentration of Phaeodaria, Rhizeria, and copepods for the 'outside-between' mask and events 1 and 2. The red horizontal line at 350±54m represents the upper limit mean of the diel vertical migration determined by ship ADCP data at the equator.

Table S1: parameters characterizing the biological carbon pump efficiency vertically

plume	Outside-between mask	event 1	event 2
E_{eff}	7 ± 28%	7 ±6%	6 ±5%
T_{eff}	31 ± 7%	29 ± 22%	40 ± 17%
b	-0.48 ± 0.5	-0.53 ± 0.5	-0.6 ± 0.9

vertically	Outside-between mask	event 1	event 2
E_{eff}	7 ± 28 %	7.5 ± 6 %	6 ± 4 %
T_{eff}	35 ± 7%	23± 28%	33± 24%
b	-0.46 ± 0.6	-0.67 ± 0.6	-0.63 ± 1